Scientific Research Publishing

Open Journal of Applied Sciences, 2025, 15(12), 4235-4259
https://www.scirp.org/journal/ojapps
ISSN Online: 2165-3925
ISSN Print: 2165-3917

Bursting and Mixed-Mode Oscillations of a Tree Trunk Structure Driven by Self and Parametric Aerodynamic Forces

Charles Adéyèm[1], Adébiyi Joseph Adéchinan[2]

[1]Doctoral School of Sciences, Technologies, Engineering and Mathematics, National University of Sciences, Technologies, Engineering and Mathematics, Abomey, Benin
[2]National Graduate School of Mathematical Engineering and Modeling, National University of Sciences, Technologies, Engineering and Mathematics, Abomey, Benin
Email: adechinan.joseph@unstim.bj

How to cite this paper: Adéyèm, C. and Adéchinan, A.J. (2025) Bursting and Mixed-Mode Oscillations of a Tree Trunk Structure Driven by Self and Parametric Aerodynamic Forces. *Open Journal of Applied Sciences*, **15**, 4235-4259.
https://doi.org/10.4236/ojapps.2025.1512274

Received: September 14, 2025
Accepted: December 26, 2025
Published: December 29, 2025

Abstract

This paper addresses the existence of bursting phenomena and mixed-mode oscillations (MMOs) in a tree trunk structure subjected to external excitation, particularly when the aerodynamic drag force is in the same direction as the flow velocity and the trunk velocity remains lower than that of the wind. A mathematical model based on Newton's second law has been developed to represent the mechanical behavior of the tree trunk. The behavior of the considered system is studied using bifurcation diagrams, Lyapunov exponent diagrams, time histories, and phase portraits. The global dynamics are explored numerically using the fourth-order Runge-Kutta method. The results reveal that our system exhibits bursting oscillations, mixed-mode oscillations, and coexisting attractors. Understanding the phenomena that appear in the system under study could help to better assess the risk of tree failure by identifying critical conditions, evaluating tree stability, and detecting potential failure modes. Both phenomena can help better predict critical conditions and improve risk management in forestry and urban environments.

Keywords

Tree Trunk, Aerodynamic Drag Force, Bursting Oscillations, Mixed-Mode Oscillations, Coexisting Attractors

1. Introduction

Trees, whose development occurs in interaction with the surrounding environment (light, temperature, nutrients, etc.), are very important for life [1]-[3]. They

play a crucial role in maintaining ecological balance and regulating the climate [4]. Despite their importance, they are unfortunately exposed to natural or human-induced threats. The interaction between wind and a tree can manifest in different ways. The wind acts on the tree by exerting a force on its branches and trunk. Wind forces are among the most critical forces that a plant must withstand. Trees, therefore, are likely to sway or twist under the influence of wind. The effects of strong winds on trees can cause them to break and damage houses, communication networks, or electrical power distribution systems [5]-[9]. Random variations in wind speed and the flexibility of branches can generate a chaotic regime and resonance vibrational phenomena [5]-[9].

In addition to these two phenomena, several other complex behaviors in dynamical systems have drawn significant attention over the past two decades, notably the bursting phenomenon [10]-[12] and the coexistence of multiple attractors in specific regions of the parameter space, both of which can influence the system's overall performance [13]. Bursting oscillations refer to a periodic alternation in the dynamic behavior of the system [14]-[17]. According to the literature, the bursting oscillation phenomenon is a particular type of nonlinear dynamics observed in certain physical, biological, or neural systems. It is characterized by an alternation between two phases in the temporal evolution of a system. This phenomenon often occurs when a system consists of two subsystems (a fast subsystem and a slow subsystem) with different time scales [18] [19]. The fast subsystem may undergo an active phase characterized by rapid oscillations followed by a stable silent phase, while the slow subsystem evolves through bifurcations [11] [20] [21]. Bursting oscillations occur in signal transduction processes and lead to a periodic switch between spiking and quiescent states [22]. Through certain studies, it is understood that the fast subsystem can alternate between spiking and quiescent states [23]. These two states characterize neuronal behaviors and are observed during the processes of encoding, decoding, and transmission in the brain [24] [25]. The bursting oscillation form, introduced by Rinzel [26] in the context of a fast-slow buster, corresponds to the transition between quiescent and spiking states. Rinzel's work has inspired numerous studies, leading to the development of several methods for predicting bursting oscillations in various forced nonlinear oscillators [18] [27]. Bursting oscillations are also studied both in oscillatory enzymatic reactions and in the context of atmospheric fluxes and bursts [28] [29]. According to [30], in dynamical systems, another type of oscillation called mixed-mode oscillation is observed. That is another type of bursting oscillations that appear in the context of slow-fast dynamic systems. The sequential alternation of large and small-amplitude oscillations, whose frequencies vary depending on the system parameters, characterizes these oscillations. The studies on the mechanism of generating MMOs have been made theoretical and numerical [31] [32]. Mixed-mode oscillations arise in many nonlinear systems such as chemical reactions [33] [34], biological systems [35] [36], electronic circuits [37] [38], and so on. Mixed-mode oscillations (MMOs) are composed of small and large ampli-

tude oscillations. They are denoted by L^s, where L and s are the large amplitude oscillations (LAOs) and small amplitude oscillations (SAOs), respectively. These oscillations are generally classified into two categories, namely primary MMOs and secondary MMOs. When the large amplitude is equal to unity ($L=1$) while the small amplitude varies from 1 to n, with n being an integer, then these oscillations are called primary MMOs. However, secondary MMOs are characterized by $L \geq 2$ and s varying from 1 to n.

The main objective of this work is to understand the emergence of bursting oscillations and mixed-mode oscillations within a tree trunk system subjected to aerodynamic loading, and to study the coexistence of attractors. The structure of this paper is as follows. In Section 2, we present the model of the tree structure. Section 3 presents the bursting phenomenon, focusing on the study of the stability and bifurcations of equilibrium points. In Section 4, we examine the occurrence of mixed-mode oscillations, and in Section 5, we analyze the coexistence of attractors in the system. The conclusion is presented in Section 6.

2. Model

Considering the tree trunk as a viscoelastic material, it can be mechanically modeled by a system consisting of a nonlinear spring and a linear dashpot connected in parallel, as illustrated by Figure 1. This mechanical analogy allows us to represent the behavior of the trunk subjected to wind excitation. Applying Newton's second law to this model, we obtain the following nonlinear dynamic equation:

$$m\frac{\mathrm{d}^2x}{\mathrm{d}t^2} = F_{ext} - F_{int} \tag{1}$$

where m represents the mass of the tree trunk, x represents the displacement of the tree trunk, F_{int} and F_{ext} denotes the internal and external forces, respectively. In this work, the internal force is defined by the following equation:

$$F_{int} = \varphi(\dot{x}) + \phi(x) \tag{2}$$

where $\varphi(\dot{x}) = d(\dot{x} - u(t))$.

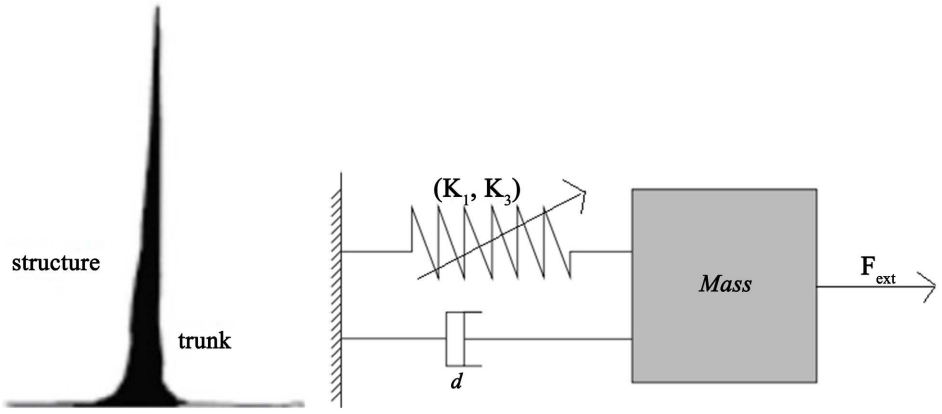

Figure 1. Dynamical model of a tree trunk: structural representation and mechanical equivalent model.

In this equation, d represents the damping coefficient, $\dot{x}$ is the speed of the tree trunk, $u(t)$ is the wind speed, and $\phi(x)$ denotes the nonlinear elastic restoring force.

In another study, [11] considered the function $\phi(x) = -kx + bx^3$ as the nonlinear elastic restoring force. The resulting equation was used to investigate burst oscillations and chaos control in pine trees. In our work, we adopt the expression $\phi(x) = -k_1 x + k_3 x^3$ with $k_1, k_3 > 0$. If we assume that the wind applies a sinusoidal excitation force of the form $F_{ext} = f\cos(\omega_2 t)$ to the tree trunk, Equation (1) becomes:

$$m\frac{\mathrm{d}^2x}{\mathrm{d}t^2} + d\frac{\mathrm{d}x}{\mathrm{d}t} - k_1 x + k_3 x^3 = f\cos(\omega_2 t) + du(t) \tag{3}$$

Equation (3) is one of the standard models used for the study of nonlinear dynamics of tree-trunk structures. It governs the motion of the tree trunk subjected to harmonic excitation due to wind and is commonly referred to as the forced damped Duffing oscillator [39]-[41].

In reality, the action of the wind on a tree and the response of the latter are complex [42]. According to [7], wind exerts a force commonly called aerodynamic drag on any tree element that is a function of the speed of the wind relative to the structure. The drag force $\Im$ on the tree can be written as:
$\Im = \kappa\rho C_D A(u(t) - \dot{x})|u(t) - \dot{x}|$.

In this work, we were interested in the specific case where the aerodynamic drag forces follow the positive direction of flow velocity, that is to say, we take $\kappa = +1$, and we stay on the case that $(u(t) - \dot{x}) > 0$, the function $(u(t) - \dot{x})^2$ stands for the fluid speed relative to the velocity. Therefore, Equation (3), influenced by fluctuating aerodynamic drag force, becomes:

$$m\ddot{x} + d\dot{x} - k_1 x + k_3 x^3 = f\cos(\omega_2 t) + du(t) + \frac{1}{2}\rho C_D A(u(t) - \dot{x})^2 \tag{4}$$

The expression for the wind speed considered is in the form:
$u(t) = U_0(1 + \eta\cos\omega_1 t)$. Unlike these authors, who assumed the wind speed to be constant, we consider in our work the case where the wind speed varies as a function of time. By introducing the dimensionless variables $X = x/L_{\max}$ and $\tau = \omega_0 t$, where $L_{\max}$ represents the length of the tree trunk and $\omega_0 = \sqrt{k_1/m}$ denotes the natural frequency of the system, we obtain, after some mathematical manipulations, when we substitute the expression for wind speed and assume that $\omega_1 = \omega_2 = \omega$, the following equation:

$$X'' + (\beta_0 + \beta_1\cos(\omega\tau) - \beta_2 X')X' - \alpha_0 - X + \alpha_3 X^3 = P\cos(\omega\tau) + h\cos(2\omega\tau) \tag{5}$$

where $\beta_0 = \frac{1}{m\omega_0}(d + \rho A C_D U_0)$, $\beta_1 = \frac{\rho A\eta C_D U_0}{m\omega_0}$, $\beta_2 = \frac{\rho A C_D L_{\max}}{2m}$,

$\alpha_3 = \frac{k_3 L_{\max}^2}{m\omega_0^2}$, $\omega = \frac{\omega_1}{\omega_0}$, $\alpha_0 = \frac{U_0}{m\omega_0^2 L_{\max}}\left(d + \frac{\rho A C_D U_0}{2}\left(1 + \frac{\eta^2}{2}\right)\right)$,

$P = \frac{1}{m\omega_0^2 L_{\max}}\left(f + \eta U_0(d + \rho A C_D U_0)\right)$, and $h = \frac{\rho A C_D \eta U_0^2}{4m\omega_0^2 L_{\max}}$.

The model considered in this work, given by Equation (5), is the same as the one we previously analyzed in an earlier publication on the chaotic behavior of a tree trunk under dynamic wind loads, with a focus on control strategies and multistability.

3. Dynamical Mechanisms of Bursting Oscillations

To describe the mechanisms responsible for the bursting oscillations in the tree trunk structure driven by self-excited and parametric aerodynamic forces, we begin by assuming that the system can be transformed into a multi-scale model composed of two different frequency components: a fast subsystem and a slow subsystem. The other state variable $X' = Y$ is introduced for convenience in the analysis. The external excitation $P\cos(\omega\tau)$ remains constant over a period T, therefore, it can be considered as a new state variable δ. Thus, Equation (5) can be rewritten in the form of a first-order differential system as follows:

$$\begin{cases} X' = Y \\ Y' = \alpha_0 + X - \alpha_3 X^3 - \left(\beta_0 + \beta_1 \dfrac{\delta}{P} - \beta_2 Y\right) Y + \delta + h\left(2\dfrac{\delta^2}{P^2} - 1\right) \end{cases} \tag{6}$$

Here, δ will be considered as the control parameter. From the perspective of slow-fast analysis, system (6) represents the fast subsystem with variables (X, Y), whereas $\dot{\delta} = -P\omega\sin(\omega\tau)$ forms the slow system. At the equilibrium point, all derivatives are zero. Thus, the determination of equilibrium points is made by setting $X' = Y' = 0$ in Equation (6). Then, as equilibrium points, we get:

$$E = \left(X^*, Y^*\right) = \left(X^*, 0\right) \tag{7}$$

where X^* verifies the following equation:

$$X^{*3} + pX^* + q = 0 \tag{8}$$

with $p = -1/\alpha_3$ and $q = -\dfrac{1}{\alpha_3}\left[\alpha_0 + \delta + h\left(2\dfrac{\delta^2}{P^2} - 1\right)\right]$.

According to the sign of Cardan discriminant $\Delta = \dfrac{p^3}{27} + \dfrac{q^2}{4}$, Equation (8) can have one, two, or three roots. So,

- if $\Delta > 0$, system (6) admits a single real equilibrium point;
- if $\Delta = 0$, system (6) admits two equilibria;
- if $\Delta < 0$, system (6) admits three equilibria.

We first linearize system (6) around the equilibrium points to analyze their stability. The Jacobian matrix of system equations given by Equation (8) at the equilibrium points E can be derived as:

$$J = \begin{pmatrix} 0 & 1 \\ 1 - 3\alpha_3 X^{*2} & -\beta_0 - \beta_1 \dfrac{\delta}{P} \end{pmatrix} \tag{9}$$

From the Jacobian matrix, the characteristic equation can be written as:

$$\lambda^2 + \lambda r_1 X^* + r_2 X^* = 0 \tag{10}$$

with $r_1 X^* = \beta_0 + \beta_1 \frac{\delta}{P}$ and $r_2 = -1 + 3\alpha_3 X^{*2}$.

According to the Routh-Hurwitz criterion for stability, the equilibrium point is asymptotically stable if and only if $r_1 > 0$ and $r_2 > 0$. The fold and Hopf bifurcations can occur when the stability conditions are changed. Thus, the following cases can be envisaged:

- $r_1 > 0$ with $\alpha_3 > 0$ and $r_2 = 0$ that is $X^* = \pm\sqrt{\frac{1}{3\alpha_3}}$, two-fold bifurcation points appear in the system.
- $r_1 = 0$ and $r_2 > 0$, both eigenvalues are pure imaginary. Then the system under consideration can present one, two, or three Hopf bifurcation points.

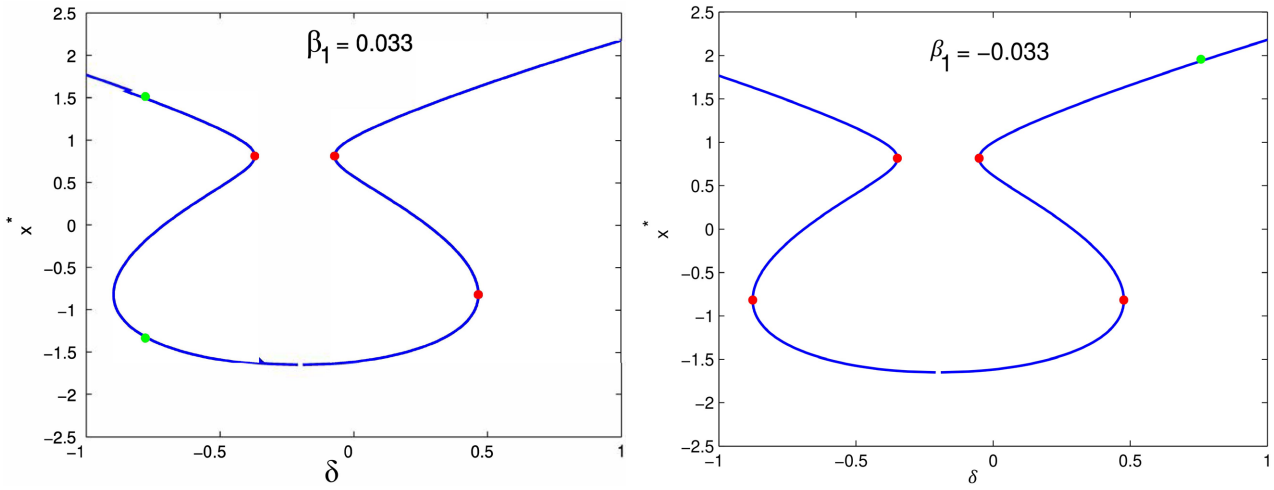

Figure 2. Evolution of equilibrium points as a function of δ for two different values of β_1 with $\alpha_3 = 0.5$, $P = 1$ and $\beta_0 = 0.025$. The green dots represent the Hopf bifurcation points, while the red dots represent the fold bifurcation points.

In order to make the stability of our system perceptible, we have a diagram represented in Figure 2. This diagram shows the evolution of the equilibrium point of a tree-trunk system for two selected values of β_1 (0.033 and −0.033) as a function of the parameter δ. The red points indicate fold bifurcations. These points mark changes in the stability of the system. The green points represent Hopf bifurcations. In this figure, the lines located between successive Hopf bifurcation points correspond to branches of stable equilibrium. The other lines of these curves are related to branches of unstable equilibrium. The characteristic bubble-shaped curves reveal a nonlinear evolution of the equilibrium point with respect to δ. These bifurcations are associated with the appearance or disappearance of oscillations in the system. For $\beta_1 = 0.033$, the curve shows a certain symmetry and the presence of bifurcations. For $\beta_1 = -0.033$, the curve exhibits a similar profile but with differences in the position or behavior of the bifurcation points. The change in the sign of influences the shape and location of the bifurcation points, indicating a sensitivity of the system's equilibrium to this parameter. The

changes in the behavior of the fold and Hopf bifurcation points suggest that the system may undergo transitions between different equilibrium states or dynamic behaviors such as oscillations. We have plotted in Figures 3-9 the time history, phase portrait, equilibrium points evolution, and transformed phase portrait for different values of the basic parameter to numerically investigate how bursting oscillations appear in our system.

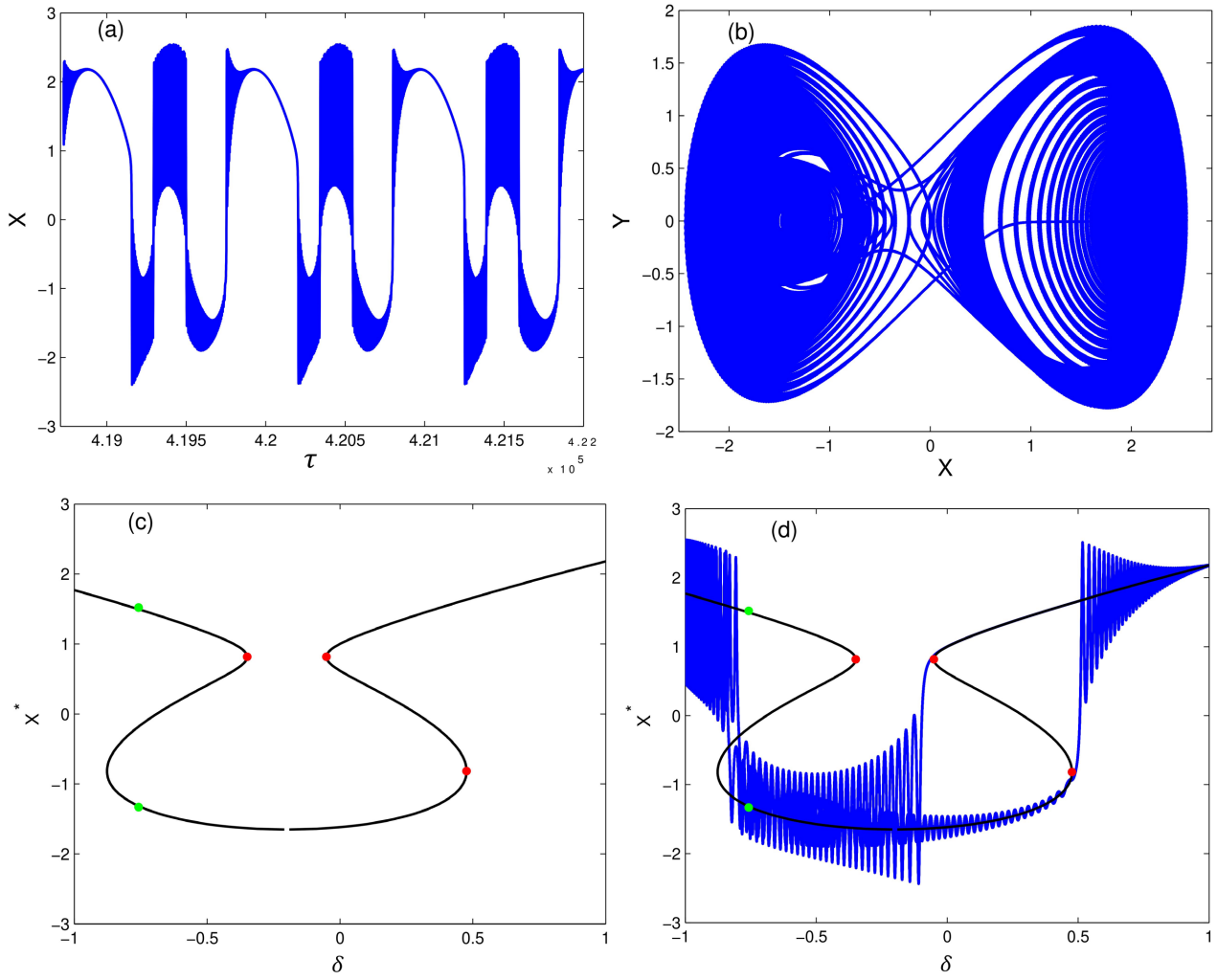

Figure 3. Bursting oscillation: (a) time history; (b) phase portrait; (c) equilibrium points evolution, and (d) transformed phase portrait with equilibrium branches. The basic parameters are $\alpha_0 = 0.75$; $\alpha_3 = 0.5$; $\beta_2 = 0.01$; $\beta_0 = 0.025$; $h = 1.25$; $\omega = 0.006$; $\beta_1 = 0.033$ and $P = 1.5$.

Figure 3(a) shows the time evolution of the displacement of a tree-trunk system. The plot displays bursting-type oscillations, characterized by periods of intense activity followed by periods of relative calm. The vertical axis represents the variable X, whose values oscillate between approximately −3 and 2 for the chosen parameters. The horizontal axis represents time τ, with values ranging from 4.19×10^5 to 4.22×10^5. This indicates that the evolution is observed over a relatively short period within a much larger time scale. The oscillations show an al-

ternation of phases in which they vary rapidly with large amplitudes, followed by phases in which they stabilize or vary more slowly. The bursts appear to repeat periodically. Figure 3(b) shows a phase portrait in the plane, where X represents the displacement of the system and Y represents its velocity. The diagram exhibits a characteristic bowtie (or butterfly) shape, typical of nonlinear dynamics involving complex behaviors such as bursting. The trajectories form loops around two main regions, indicating oscillatory phases with transitions between different dynamical states. The system alternates between phases of intense activity (bursts) and phases of rest or low activity. To more easily understand the mechanism of this explosive oscillation, we have transformed the phase portrait of Figure 3(b) into Figure 3(d). The variable δ represents the control parameter of the system, and the variable X^* represents the equilibrium point. In this figure, we assume that the trajectory starts from a point of the rightmost upper stable equilibrium branch (at $\delta = 1$), where the attractor is categorized as the stable fixed point. As δ decreases, a repetitive spiking movement with large amplitude is observed along its domain of attraction. As δ continues to decrease and reaches the fold bifurcation point at $\delta = 0.1$, the trajectory jumps to the lower stable equilibrium branch, and the spiking state movement is created. As δ further decreases and reaches the Hopf bifurcation point located $\delta = -0.75$, the trajectory jumps to the second upper stable equilibrium branch, generating a repetitive spiking state movement. When δ increases and passes through the Hopf bifurcation point, the quiescent state movement is created. When δ continues to increase, the trajectory jumps at $\delta = 0.45$ into the first upper stable equilibrium branch and passes through the fold bifurcation point and the repetitive spiking state movement reappears. As δ increases, the trajectory returns to the starting point when $\delta = 1$. This bursting oscillation can be classified as an asymmetric fold/Hopf-fold bursting type.

Figure 4(b) shows the time evolution of a bursting-type oscillation in the system modeling a tree trunk. The system exhibits periodic episodes of large-amplitude oscillations (with a range approximately from −2.5 to 2), followed by phases where the amplitude decreases. The bursts repeat regularly along the time axis, revealing a cyclic dynamic. Oscillates with positive peaks close to 2 and minima close to −2.5. The pattern repeats periodically, and the shape of the oscillations shows rapid transitions between extrema, which suggests a bursting oscillation cycle. The phase portrait (see Figure 4(b)) shows that the attractors oscillate around two equilibrium points. This portrait is mainly characterized by its hourglass shape. The plot forms a symmetric structure resembling an hourglass, with tight loops at the center (near $X = 0$) that widen toward the extremities (±2). This reveals oscillations with phases of large excursions in displacement/velocity, followed by returns to a more confined region. Near the center ($X = 0$), one observes tight loops or spirals indicating small-amplitude oscillations around an equilibrium point. Moving away from the center, the trajectories widen and display complex patterns with crossings, corresponding to phases of larger-amplitude oscillations. The transformed phase portrait is plotted in Figure 4(d) to re-

veal the mechanism of bursting oscillation. This Figure shows the transformed phase portrait with equilibrium branches for a bursting-type oscillation in a tree-trunk system. The parameter appears to control the transition between different dynamical regimes. In this figure, we assume that the trajectory starts from a point of the rightmost upper stable equilibrium branch (at $\delta = 1.5$) and decreases. As δ continues to decrease and reaches the fold bifurcation point at $\delta = 0$, the trajectory jumps to the lower stable equilibrium branch, and the spiking state movement is observed. When δ increases from −1.5 and passes through the Hopf bifurcation point and reaches the fold bifurcation point, the trajectory jumps at $\delta = -0.75$ into the lower stable equilibrium branch, and the spiking state movement reappears. As δ continues to increase and reaches the fold bifurcation point, the trajectory jumps into the upper stable equilibrium branch and returns to the starting point at $\delta = 1.5$, the spiking state is observed. This bursting oscillation can be classified as asymmetric fold-Hopf/Hopf-fold-fold bursting.

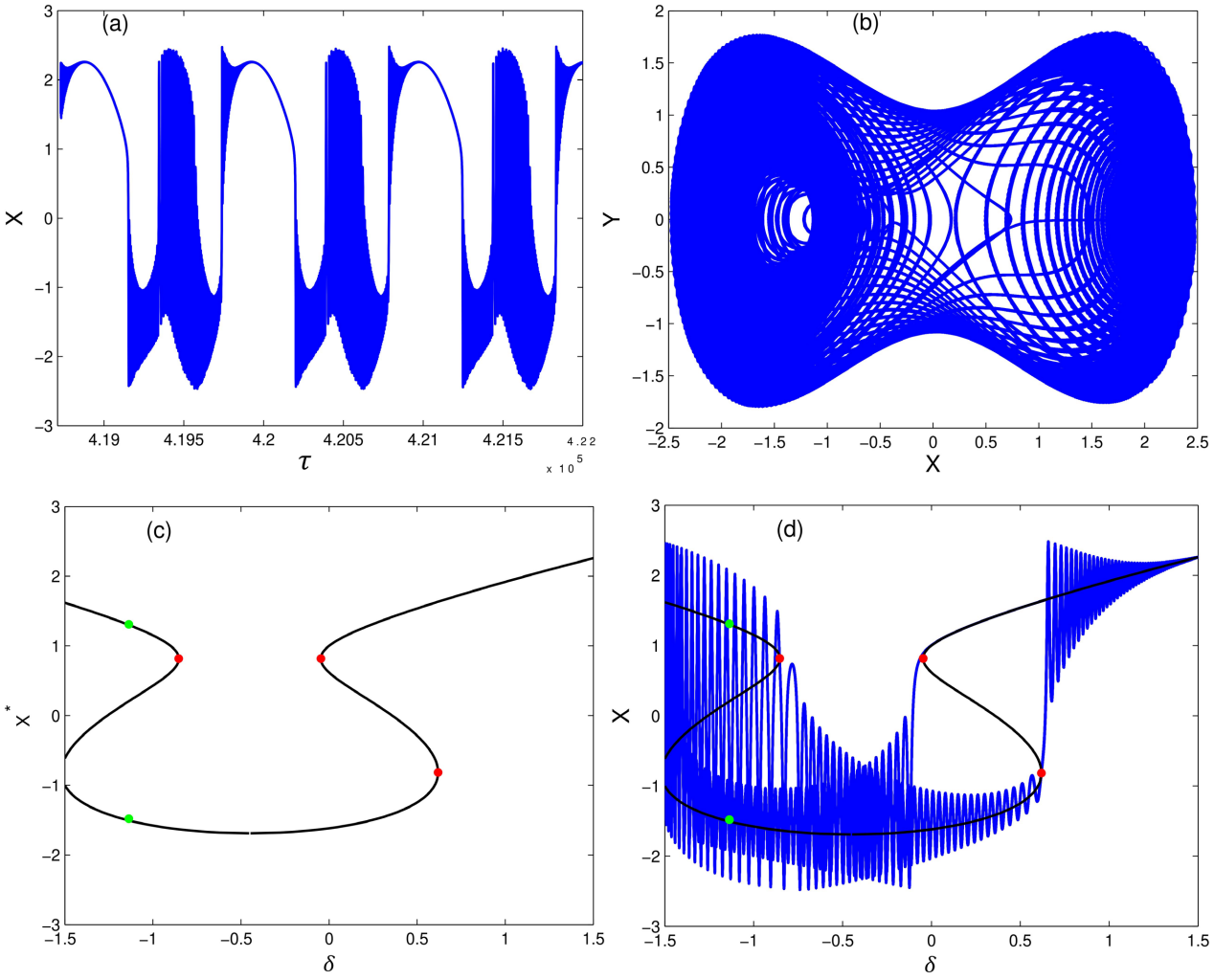

Figure 4. Bursting oscillation: (a) time history; (b) phase portrait; (c) equilibrium points evolution, and (d) transformed phase portrait with equilibrium branches. The basic parameters are $\alpha_0 = 0.75$; $\alpha_3 = 0.5$; $\beta_2 = 0.01$; $\beta_0 = 0.025$; $h = 1.25$; $\omega = 0.006$; $\beta_1 = 0.033$ and $P = 2$.

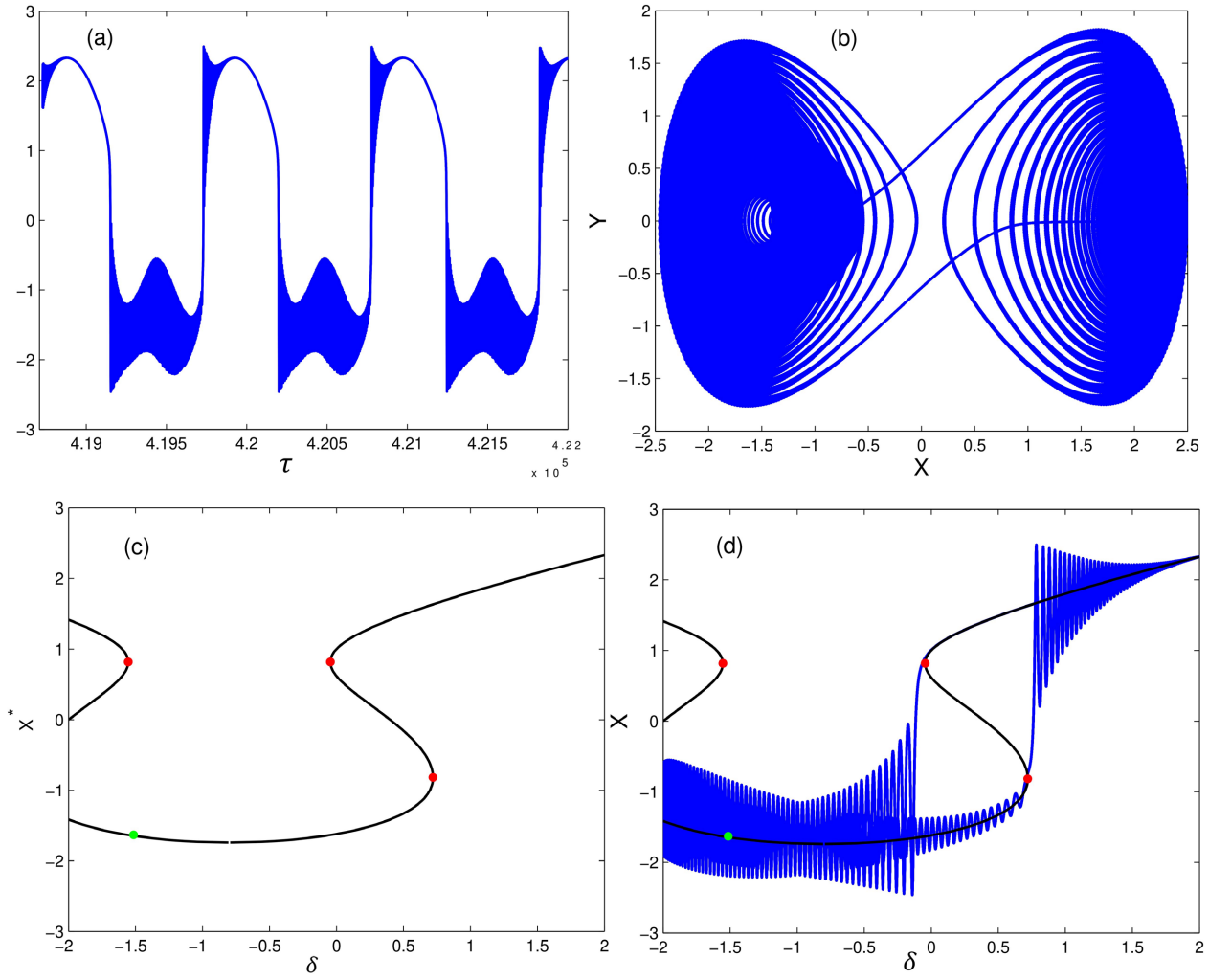

Figure 5. Bursting oscillation: (a) time history; (b) phase portrait; (c) equilibrium points evolution, and (d) transformed phase portrait with equilibrium branches. The basic parameters are $\alpha_0 = 0.75$; $\alpha_3 = 0.5$; $\beta_2 = 0.01$; $\beta_0 = 0.025$; $h = 1.25$; $\omega = 0.006$; $\beta_1 = 0.033$ and $P = 5$.

Figure 5(a) shows the time evolution of a bursting-type oscillation in a tree-trunk system. The plot displays a bursting oscillation, characterized by periods of intense activity (the bursts) followed by periods of low activity or silence. The horizontal axis represents time (in seconds, with a scale in seconds), indicating that the observed phenomena occur on a very short timescale. The vertical axis shows the amplitude of the oscillations, ranging from approximately −2.5 to 2.5. The oscillations have a particular shape with pronounced peaks and troughs. Repetitive bursting cycles can be observed, with active phases in which the amplitude varies rapidly; the bursts exhibit a structure with maxima and minima that repeat periodically. **Figure 5(b)** illustrates the nonlinear dynamics of a tree trunk in a bursting regime. Two sets of closed trajectories can be observed, forming a symmetric "butterfly" structure. Each set corresponds to a fast oscillatory phase around a quasi-stable state, while the central area represents the rapid transitions between these two regimes. This behavior highlights the coexistence of two attractors and

the presence of bistable transitions, characteristic of bursting phenomena. Physically, it reflects the alternation between calm phases and intense oscillation phases of the trunk, induced by slow variations in wind force. In order to reveal the mechanism of this bursting oscillation, the transformed phase portrait is plotted in Figure 5(d). The system follows the stable branch until it reaches a bifurcation point where stability is lost. At that moment, the system abruptly jumps to another stable branch, generating a rapid oscillation (burst). From this figure, we assume that the trajectory starts from $\delta = 2$ and moves through the upper stable equilibrium branch where the spiking state is observed when δ decreases. As δ continues to decrease and reaches the fold bifurcation point, the trajectory jumps into the lower stable equilibrium branch where the spiking state is observed. As δ increases from -2 passing through the Hopf bifurcation point and reaches the fold bifurcation point, the spiking state disappears, and the quiescent state appears. As δ continues to increase and reaches the fold bifurcation point, the trajectory jumps at $\delta = 0.75$ into the upper stable equilibrium branch, and the repetitive spiking state movement appears. The trajectory returns to its starting point. Then, this bursting oscillation can be classified as an asymmetric fold/Hopf-fold hysteresis bursting type.

Figure 6(a) shows the time evolution of the variable. One observes repetitive cycles characterized by phases of intense activity where X reaches values close to 3, followed by phases of low activity during which X quickly drops toward -2 and then gradually rises again. The bursts are periodic and exhibit a marked asymmetry: a rapid rise toward the peak followed by a more gradual descent with a "tail" toward negative values before bouncing back. This dynamic reveals nonlinear behavior with abrupt transitions between active and calm phases, potentially linked to mechanical mechanisms within the tree trunk. Figure 6(b) shows the phase portrait of the tree-trunk system, revealing complex bursting-type dynamics characterized by nonlinear oscillations between two distinct regions of the phase space. The butterfly shape of the diagram indicates an alternation between phases of intense activity and phases of low activity, with rapid transitions between these states. The tight loops at the center of the diagram suggest abrupt changes in velocity, while the outer parts of the loops show slower excursions or bursts. In order to reveal the mechanism of this bursting oscillation, the transformed phase portrait is plotted. Figure 6(d) shows the transformed phase portrait. An S-shaped structure formed by the black curve (the equilibrium point curve) can be observed, with two red points marking critical transitions. From this figure, we assume that the trajectory starts from $\delta = 5$ and moves through the upper stable equilibrium branch when δ decreases. As δ continues to decrease through the fold bifurcation point, the trajectory jumps into the lower stable equilibrium branch, and the spiking state is created. When δ increases from -5 and passes through the Hopf bifurcation point, the spiking state disappears. As δ increases and reaches the fold bifurcation point, the trajectory jumps into the upper stable equilibrium branch, and the spiking state appears. As δ continues

to increase to 5, the trajectory returns to its starting point. Then, this bursting oscillation can be classified as an asymmetric fold/Hopf-fold hysteresis bursting type.

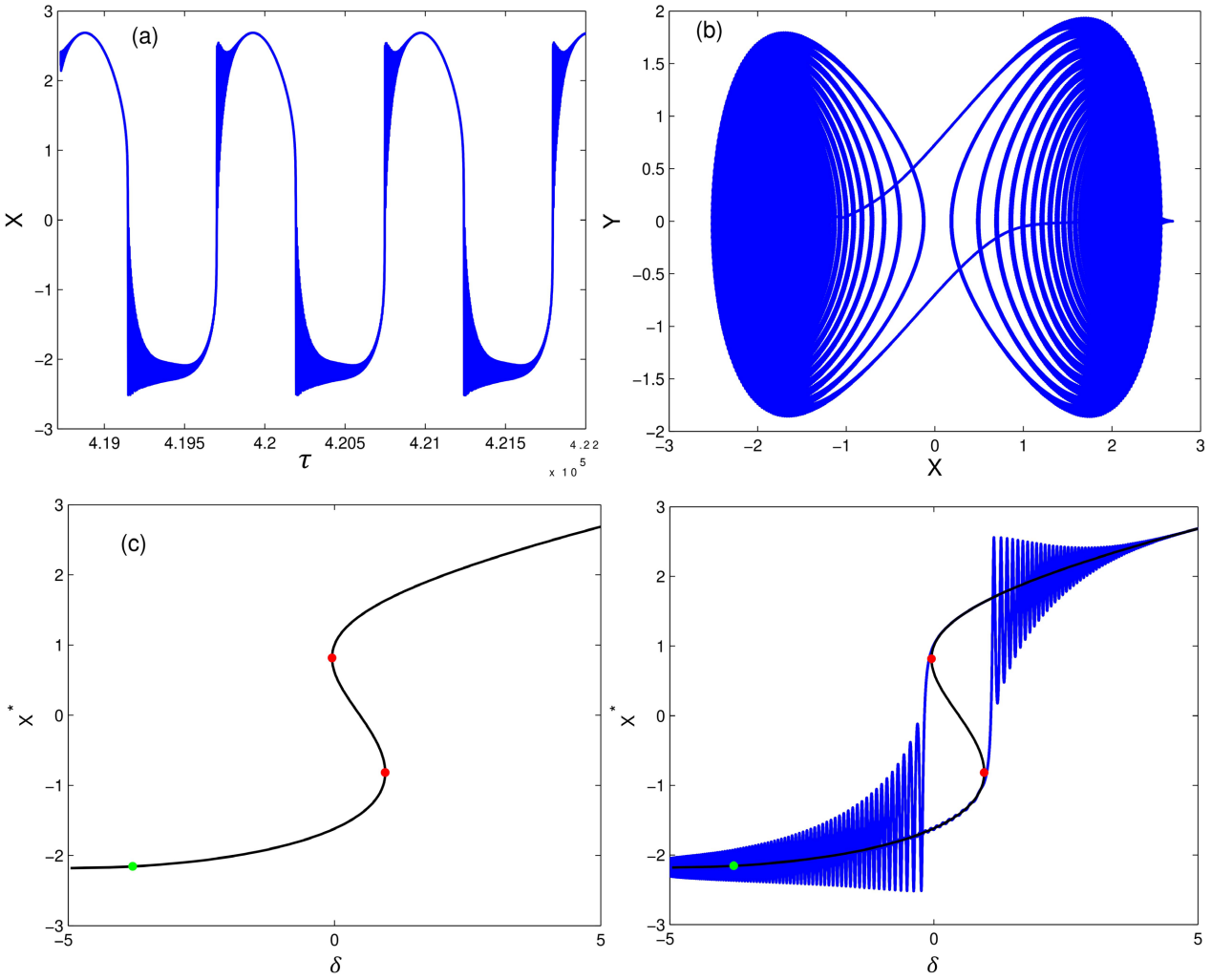

Figure 6. Bursting oscillation and with the parameters of **Figure 2**: (a) time history; (b) phase portrait; (c) equilibrium points evolution, and (d) transformed phase portrait with equilibrium branches. The basic parameters are $\alpha_0 = 0.75$; $\alpha_3 = 0.5$; $\beta_2 = 0.01$; $\beta_0 = 0.025$; $h = 1.25$; $\omega = 0.006$; $\beta_1 = -0.033$ and $P = 1$.

Figure 7(a) shows the time evolution of a bursting-type oscillation in a tree-trunk system. The variable oscillates periodically, with bursts characterized by rapid and large-amplitude excursions followed by phases in which it returns to values close to zero. The oscillations exhibit an alternation between high peaks and low-amplitude periods, suggesting nonlinear dynamics in which the system switches between phases of intense activity and phases of relative calm. **Figure 7(b)** shows a blue region representing the set of possible system trajectories in the phase space, with corresponding displacement and velocity. The shape of this region suggests a confinement zone for the trajectories around a central point, indicating a tendency of the system to evolve within a limited region of phase space. The presence of a point at the center could represent an equilibrium point or an

area of low dynamical activity. This phase portrait is typical of bursting behavior, where the system alternates between phases of intense activity and resting phases. In order to reveal the mechanism of this bursting oscillation, the transformed phase portrait is plotted. Figure 7(d) presents the phase portrait showing a bifurcation with equilibrium branches represented by black lines, surrounded by a blue region that indicates a zone of stability or attraction for the system's trajectories. The presence of such a bifurcation suggests that the system can move from a stable state to a complex oscillation regime of bursting type in function of δ. From this figure, we assume that the trajectory starts from $\delta = 1$ and moves through the upper stable equilibrium branch where the spiking state is observed when δ decreases. As δ continues to decrease through the Hopf bifurcation point and reaches the fold bifurcation point, the trajectory jumps into the lower stable equilibrium branch. As δ continues to decrease and

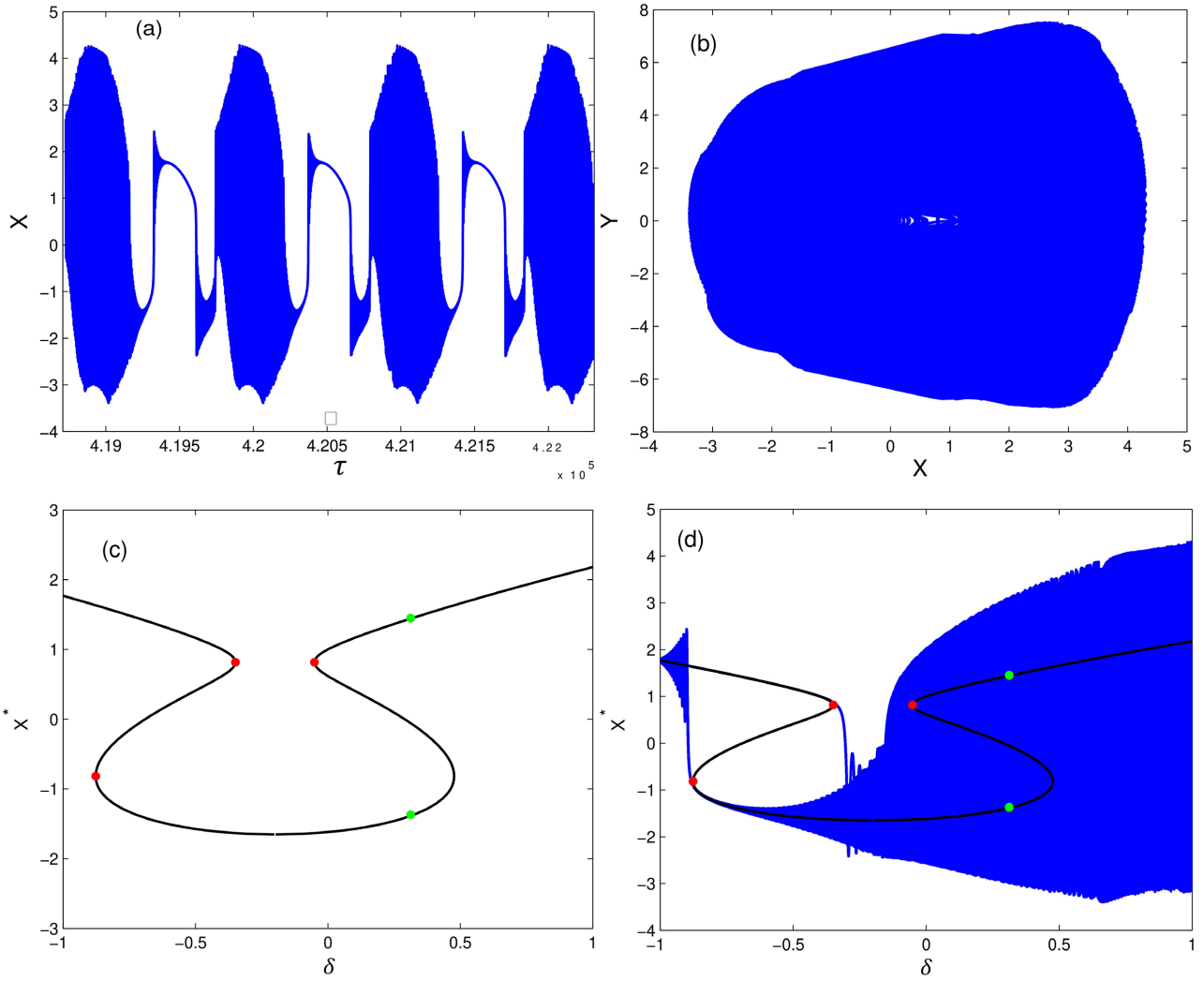

Figure 7. Evolution of equilibrium points as a function of δ for two different values of β_1. The green dots represent the Hopf bifurcation points while the red dots represent the fold bifurcation points. The basic parameters are $\alpha_0 = 0.75$; $\alpha_3 = 0.5$; $\beta_2 = 0.01$; $\beta_0 = 0.025$; $h = 1.25$; $\omega = 0.006$; $\beta_1 = -0.033$ and $P = 1.5$.

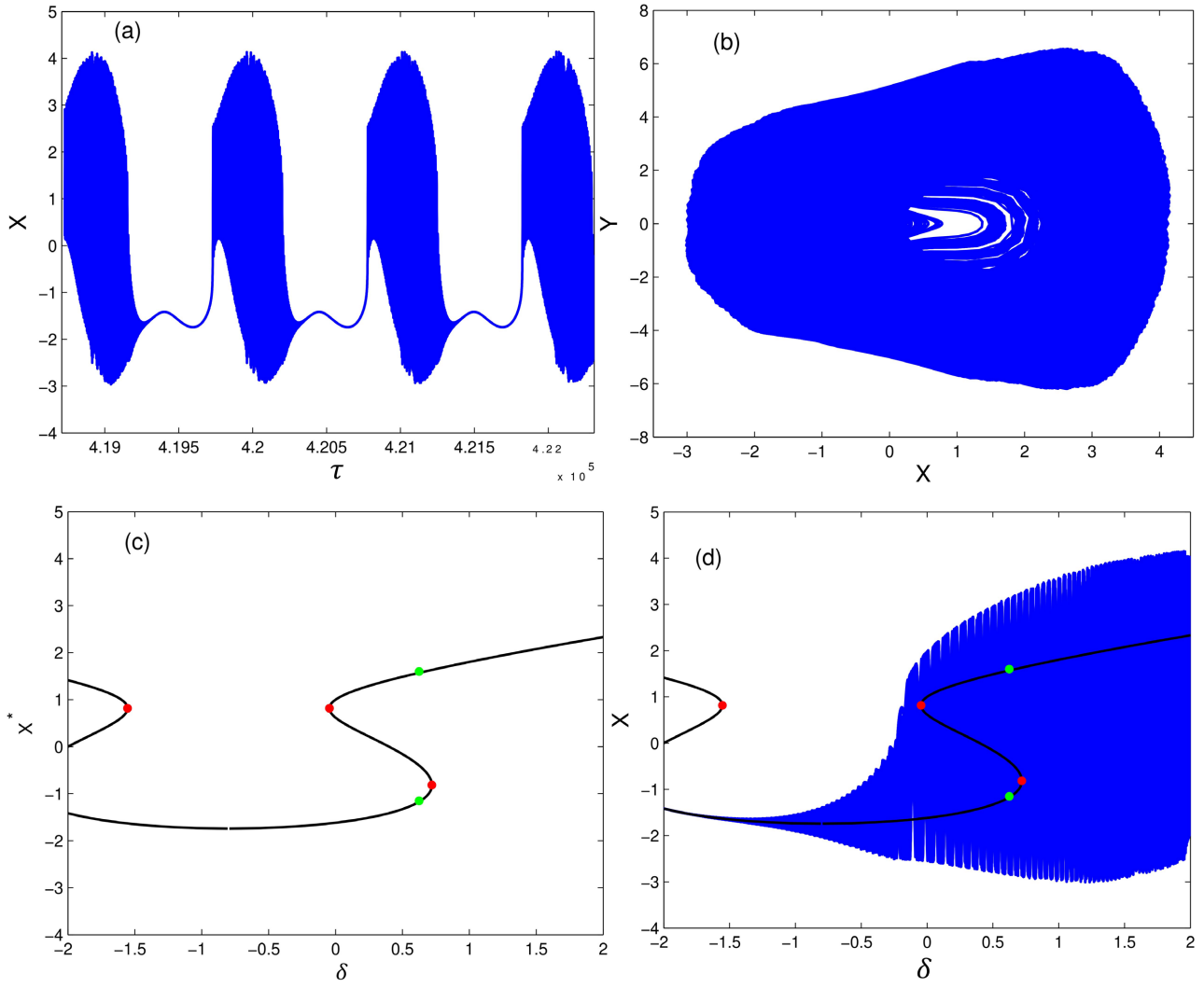

Figure 8. Bursting oscillation and with the parameters of **Figure 2**: (a) time history; (b) phase portrait; (c) equilibrium points evolution, and (d) transformed phase portrait with equilibrium branches. The basic parameters are $\alpha_0 = 0.75$; $\alpha_3 = 0.5$; $\beta_2 = 0.01$; $\beta_0 = 0.025$; $h = 1.25$; $\omega = 0.006$; $\beta_1 = -0.033$ and $P = 2$.

reaches the fold bifurcation point, the trajectory jumps into the left upper stable equilibrium branch where the spiking state is observed. When δ increases from -1 and reaches the fold bifurcation point, the trajectory jumps back into the lower stable equilibrium branch and the spiking state reappears. When δ continues to increase to 1, the trajectory returns to its starting point by maintaining the spiking state. Then, this bursting oscillation can be classified as an asymmetric Hopf-fold-fold/fold-Hopf type.

Figure 8(a) shows a series of periodic oscillations characterized by phases of intense activity followed by periods of low activity. The bursts appear as regular peaks with high amplitudes, alternating with phases where the amplitude decreases significantly. **Figure 8(b)** shows a dense blue region representing the set of possible trajectories of the system in phase space. At the center of the diagram, a characteristic white "arrowhead" shape indicates a zone where trajectories converge

or focus toward a specific cycle or point. The trajectories seem to spiral around this central area, suggesting complex oscillatory behavior typical of bursting phenomena. This reveals nonlinear dynamics in which the system alternates between phases of intense activity and phases of rest or low activity, highlighting the richness of interactions between displacement and velocity in this system. In order to reveal the mechanism of this bursting oscillation, the transformed phase portrait is plotted. **Figure 8(d)** presents the transformed phase portrait. The diagram shows an extended blue region representing a zone of oscillatory behavior of the system as a function of the parameter δ. A bifurcation is observed around $\delta = 0$, where the system's behavior appears to change significantly, transitioning from one regime to another with oscillatory characteristics potentially of the bursting type. This phase portrait highlights the system's sensitivity to variations in the parameter, influencing transitions between equilibrium states and phases of complex oscillations. This bursting oscillation can be classified as an asymmetric Hopf-fold/Hopf-fold type.

Figure 9(a) shows a series of periodic oscillations characterized by phases of intense activity (bursting) followed by low-amplitude periods. The plot illustrates the evolution of the variable as a function of time, with oscillations that appear to repeat in a regular manner. The peaks of these oscillations exhibit slightly varying amplitudes but maintain an overall periodicity, suggesting a cyclic dynamic behavior in the system under consideration. **Figure 9(b)** illustrates the phase portrait, revealing complex dynamics characterized by cycles of displacement and velocity. The diagram shows two main lobes that are symmetric with respect to the origin, indicating alternating oscillatory phases in which the system undergoes periods of intense activity (bursting) followed by calmer phases. The trajectories form nested loops within each lobe, suggesting repeated transitions between states of high and low displacement and velocity. This structure reflects nonlinear behavior typical of systems exhibiting bursting phenomena, where coupling between displacement and velocity generates complex dynamic patterns. In order to reveal the mechanism of this bursting oscillation, the transformed phase portrait is plotted. **Figure 9(d)** presents the transformed phase portrait, revealing key characteristics of the system's dynamics. The phase portrait shows a U-shaped curve. The ends of the U-shaped curve display areas of strong variation, suggesting rapid transitions between system states. The equilibrium branches frame a region where the system may exhibit complex oscillatory behavior, typical of bursting phenomena. This diagram highlights the coexistence of phases of intense activity and phases of rest in the dynamics of the tree-trunk system. From this figure, we assume that the trajectory starts from $\delta = 2.25$ and moves through the upper stable equilibrium branch when δ decreases. As δ continues to decrease and reaches the fold bifurcation point at $\delta = 1.25$, the trajectory jumps into the lower stable equilibrium branch. As δ increases from -1.5 passing through the Hopf bifurcation point and fold bifurcation point, the quiescent state is not observed. When δ evolves, the tra-

jectory jumps into the spiking state. As δ continues to decrease from −2.25, the trajectory returns to its starting point. Then, this bursting oscillation can be classified as an asymmetric fold-Hopf-fold/Hopf-fold-fold type.

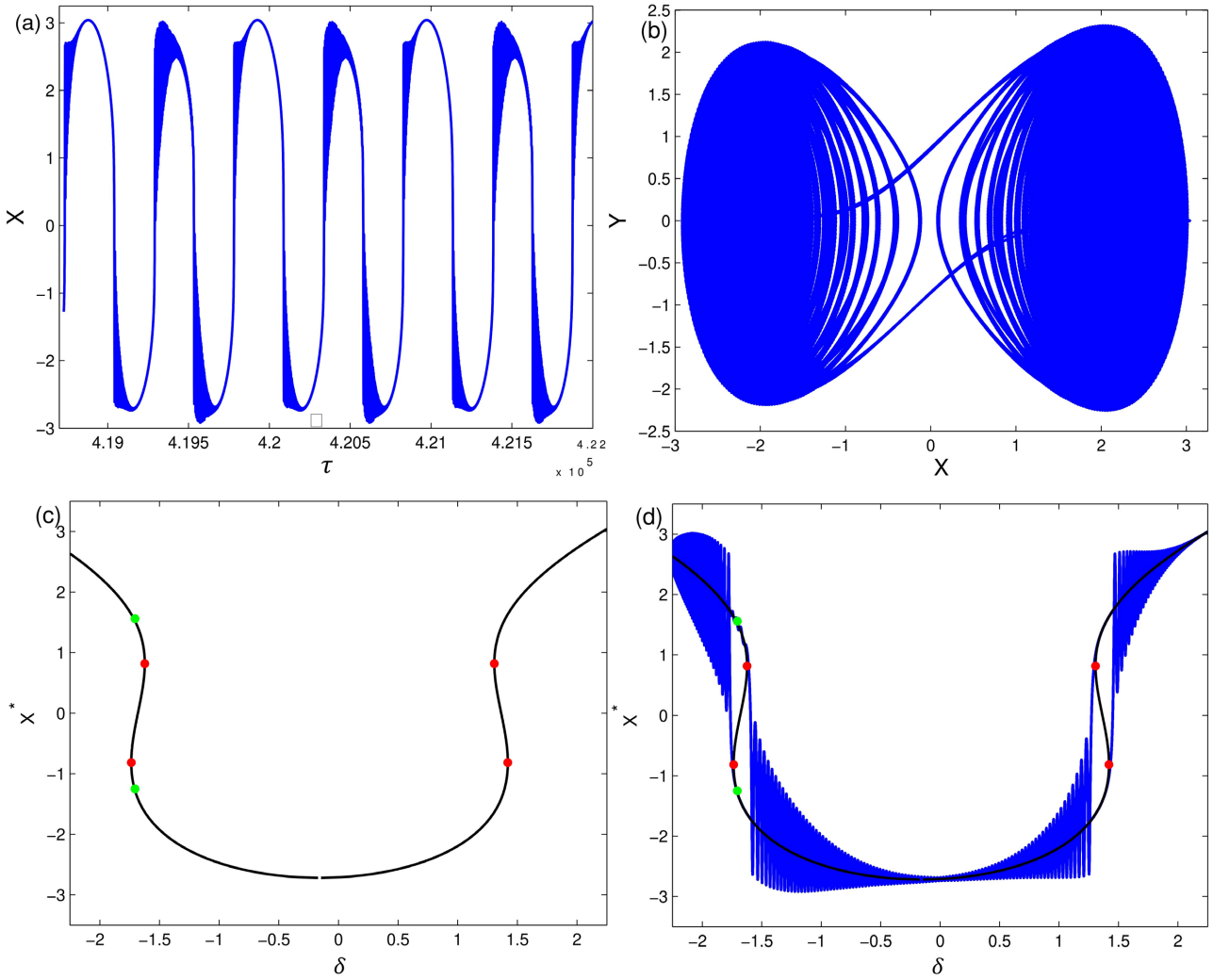

Figure 9. Bursting oscillation and with the parameters of **Figure 2**: (a) time history; (b) phase portrait; (c) equilibrium points evolution, and (d) transformed phase portrait with equilibrium branches. The basic parameters are $\alpha_0 = 0.75$; $\alpha_3 = 0.5$; $\beta_2 = 0.01$; $\beta_0 = 0.025$; $h = 1.25$; $\omega = 0.006$; $\beta_1 = -0.033$ and $P = 5$.

4. Bursting and Mixed-Mode Oscillations

Our objective in this section is to understand the emergence of bursting and mixed-mode oscillations within a tree trunk system subjected to hydrodynamic loading. To achieve this, we employed the fourth-order Runge-Kutta algorithm to numerically construct bifurcation diagrams and their corresponding Lyapunov exponent diagrams. As depicted in **Figure 10** and **Figure 11**, these bifurcation diagrams illustrate the system's behavior as the control parameter ω varies, with β_1 values of −0.033 and −0.009, respectively. The remaining parameter values used for these simulations were $\alpha_0 = 0.75$, $\alpha_3 = 0.5$, $\beta_0 = 0.025$; $\beta_2 = 0.015$;

$f = 2$, $h = 0.5$, and the initial conditions were $X(0) = 0.5$ and $Y(0) = 0.5$.

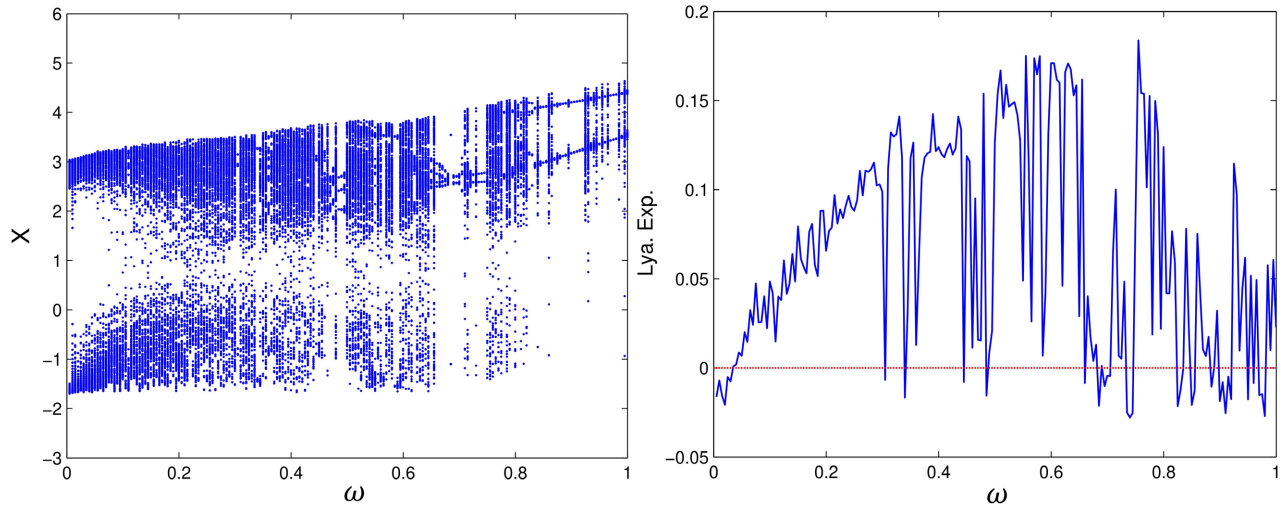

Figure 10. Bifurcation diagrams and its corresponding Lyapunov exponent versus ω of the system with the parameter values $\alpha_0 = 0.75$; $\alpha_3 = 0.5$; $\beta_0 = 0.025$; $\beta_2 = 0.015$; $f = 2$; $h = 0.5$; $\beta_1 = -0.033$.

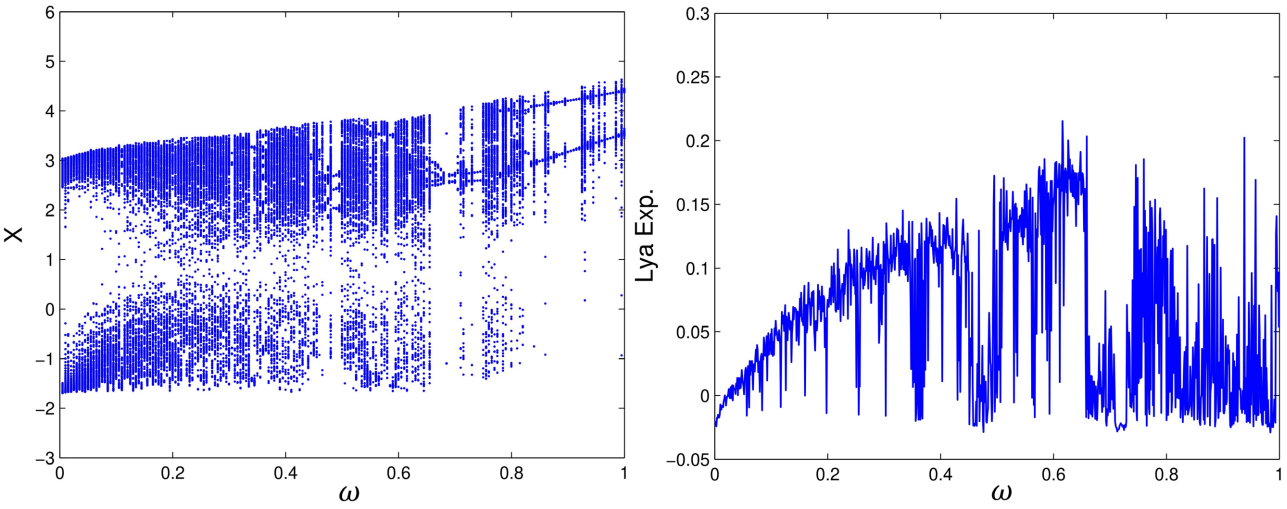

Figure 11. Bifurcation diagrams and its corresponding Lyapunov exponent versus ω of the system with the parameter values $\alpha_0 = 0.75$; $\alpha_3 = 0.5$; $\beta_0 = 0.025$; $\beta_2 = 0.015$; $f = 2$; $h = 0.5$; $\beta_1 = -0.009$.

Figure 10 and Figure 11 reveal that the system exhibits periodic mixed-mode oscillations and chaotic bursting oscillations, alongside reverse periodic bifurcations. To further illustrate the diverse oscillation types predicted by the bifurcation diagrams in Figure 10, we've plotted various phase portraits of the system in Figure 12 for different values of ω. This figure specifically demonstrates chaotic bursting oscillations at $\omega = 0.1$, 0.52, 0.622. Additionally, the system displays primary periodic mixed-mode oscillations of varying topologies. Notably, at $\omega = 0.621$, the system displays transitions from $1^1 1^2$ mixed-mode oscillations (MMOs) to chaos, and 1^2MMOs to chaos are also observed. To further investigate the behavior predicted by the bifurcation diagram in Figure 10, Figure 13 displays phase portraits of sev-

eral periodic attractors. From these portraits, we observe the system exhibiting a variety of secondary mixed-mode oscillations (MMOs), thereby uncovering their distinct routes to chaos.

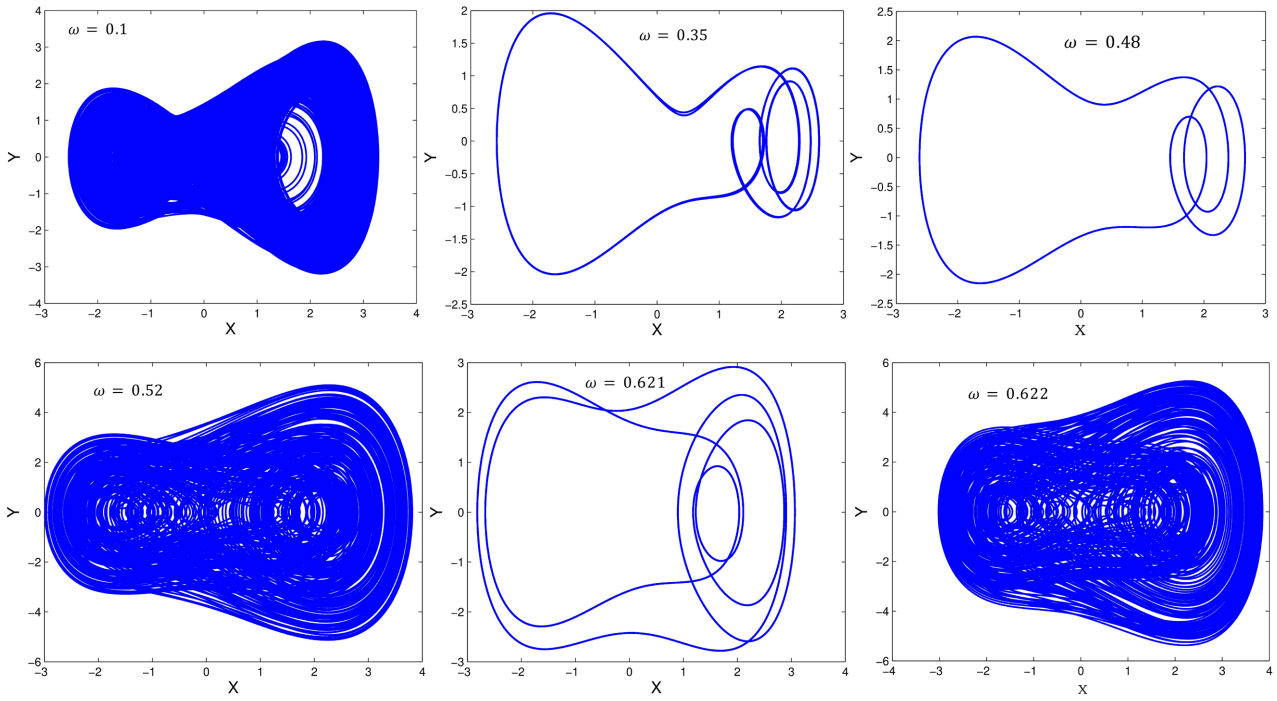

Figure 12. Several phase portraits of the system illustrate chaotic and periodic bursting-type oscillations, as well as mixed-mode oscillations for several values of ω with the parameters of Figure 10.

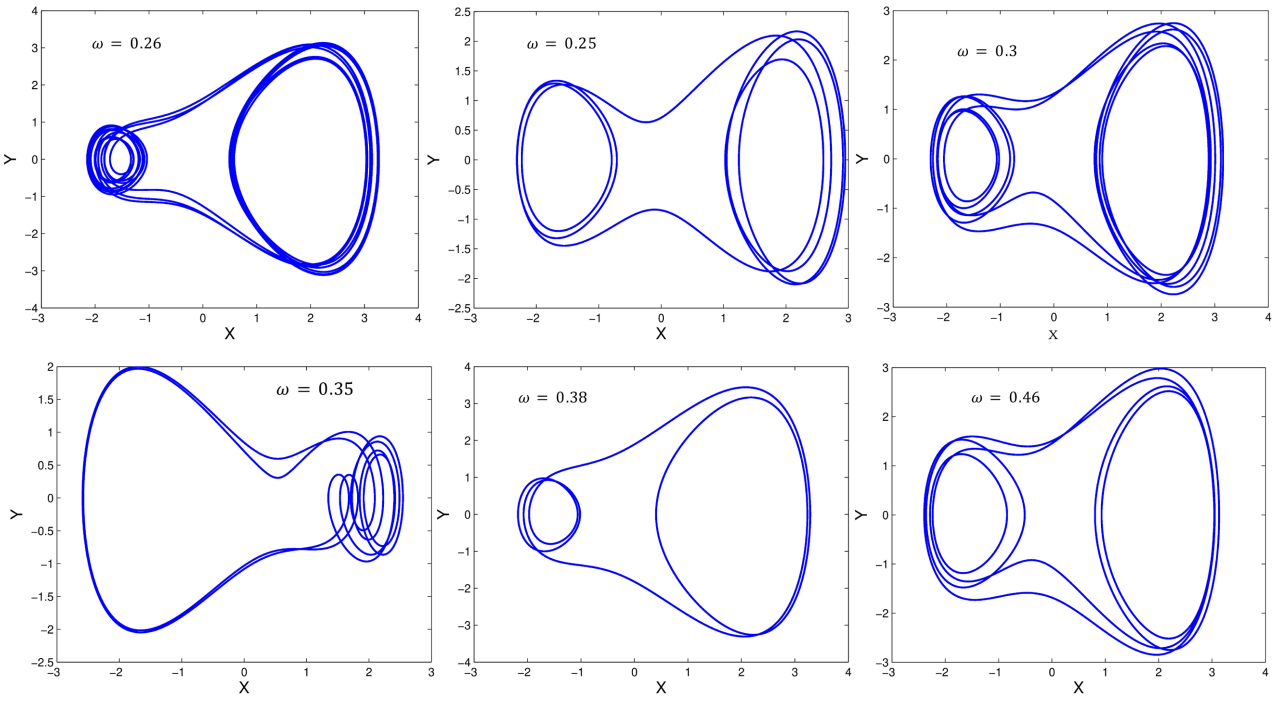

Figure 13. Several phase portraits of the system exhibit secondary periodic mixed-mode oscillations for certain values of ω with the parameters of Figure 10.

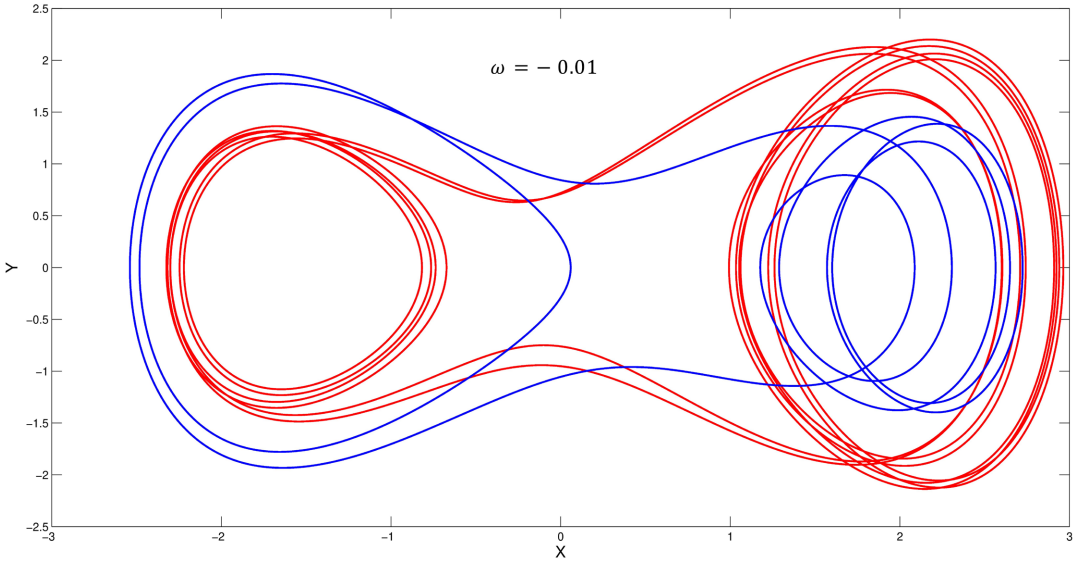
$\omega = -0.01$
Y
X

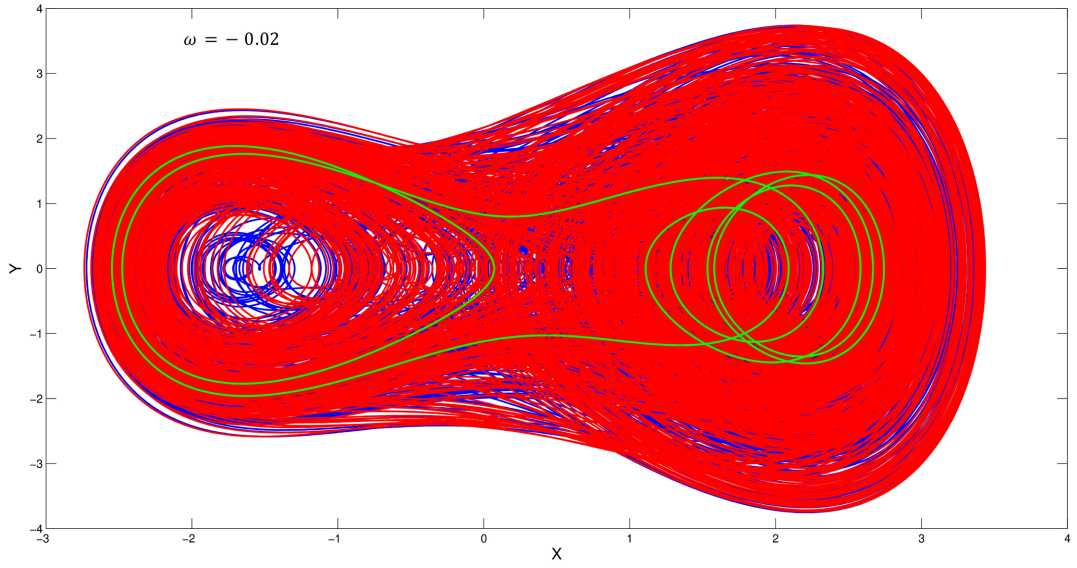
$\omega = -0.02$
Y
X

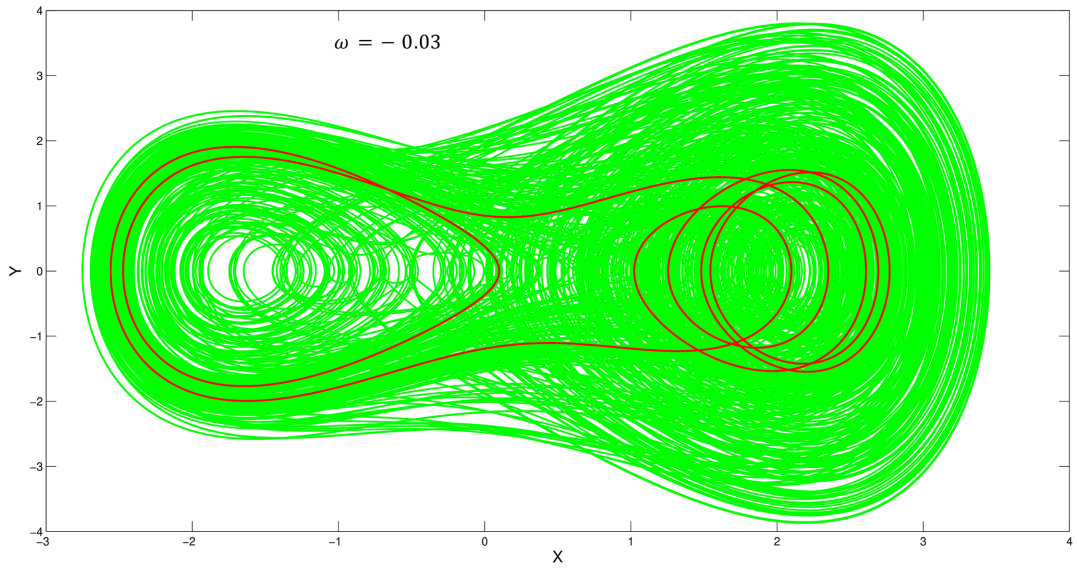
$\omega = -0.03$
Y
X

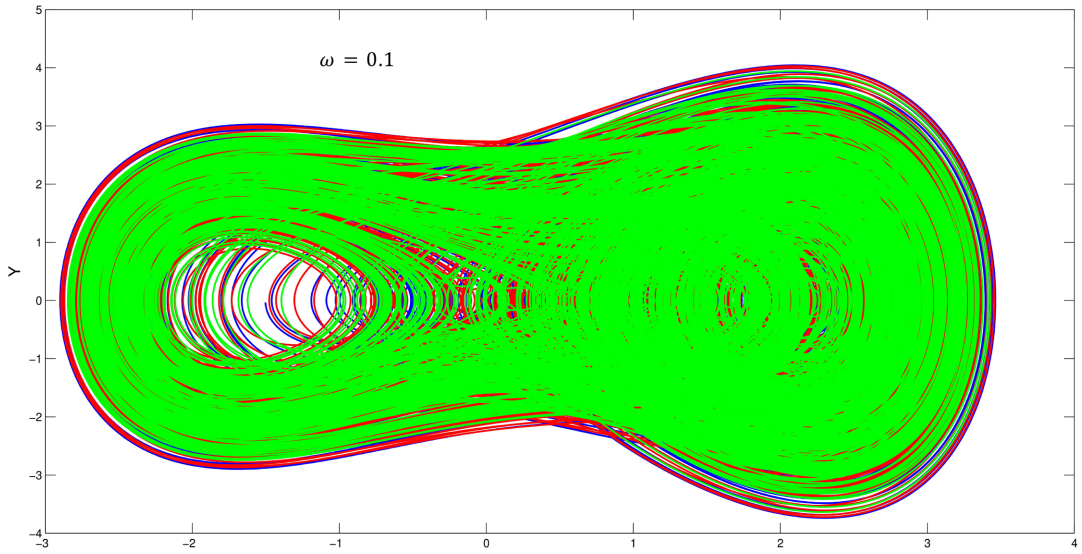

Figure 14. Coexisting attractor behaviors of the system with four different values of β_1 with $\omega = 0.25$. The other parameter values of **Figure 9** are kept constant.

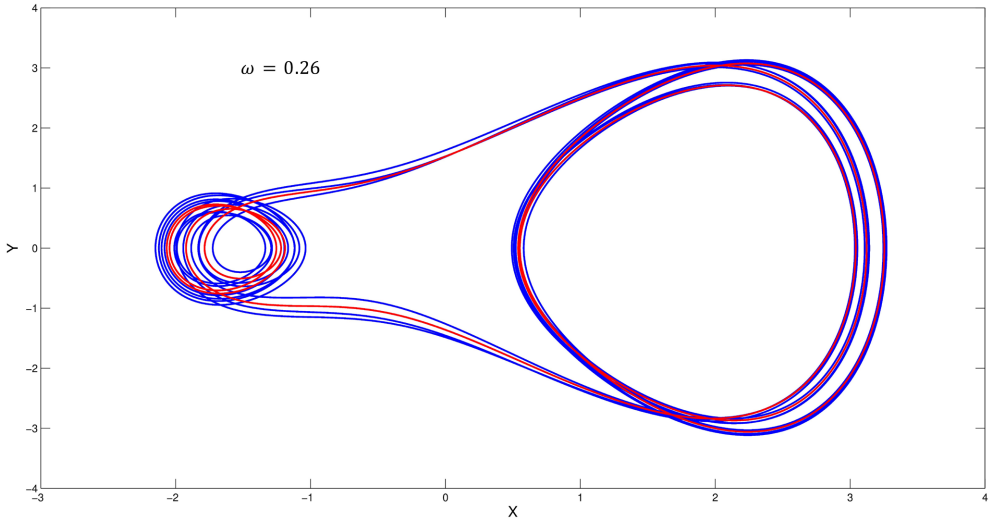

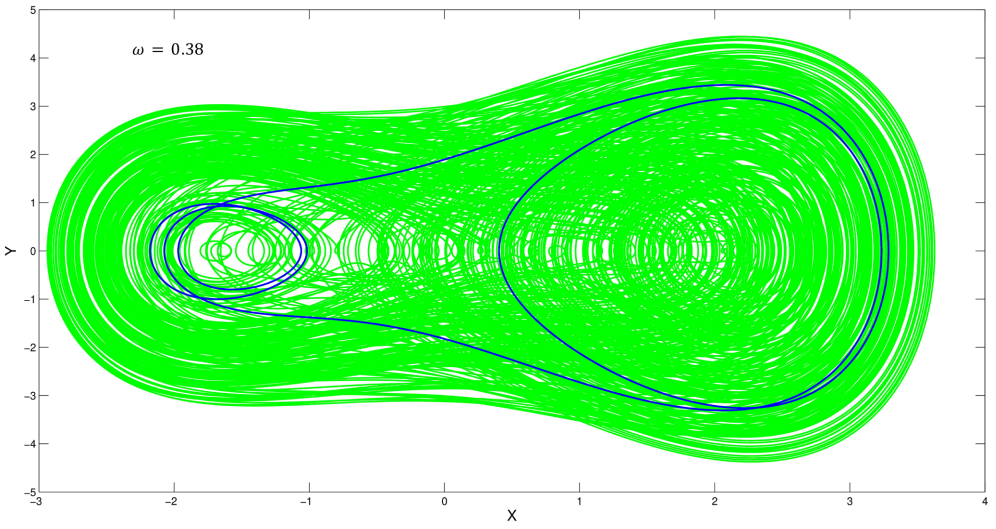

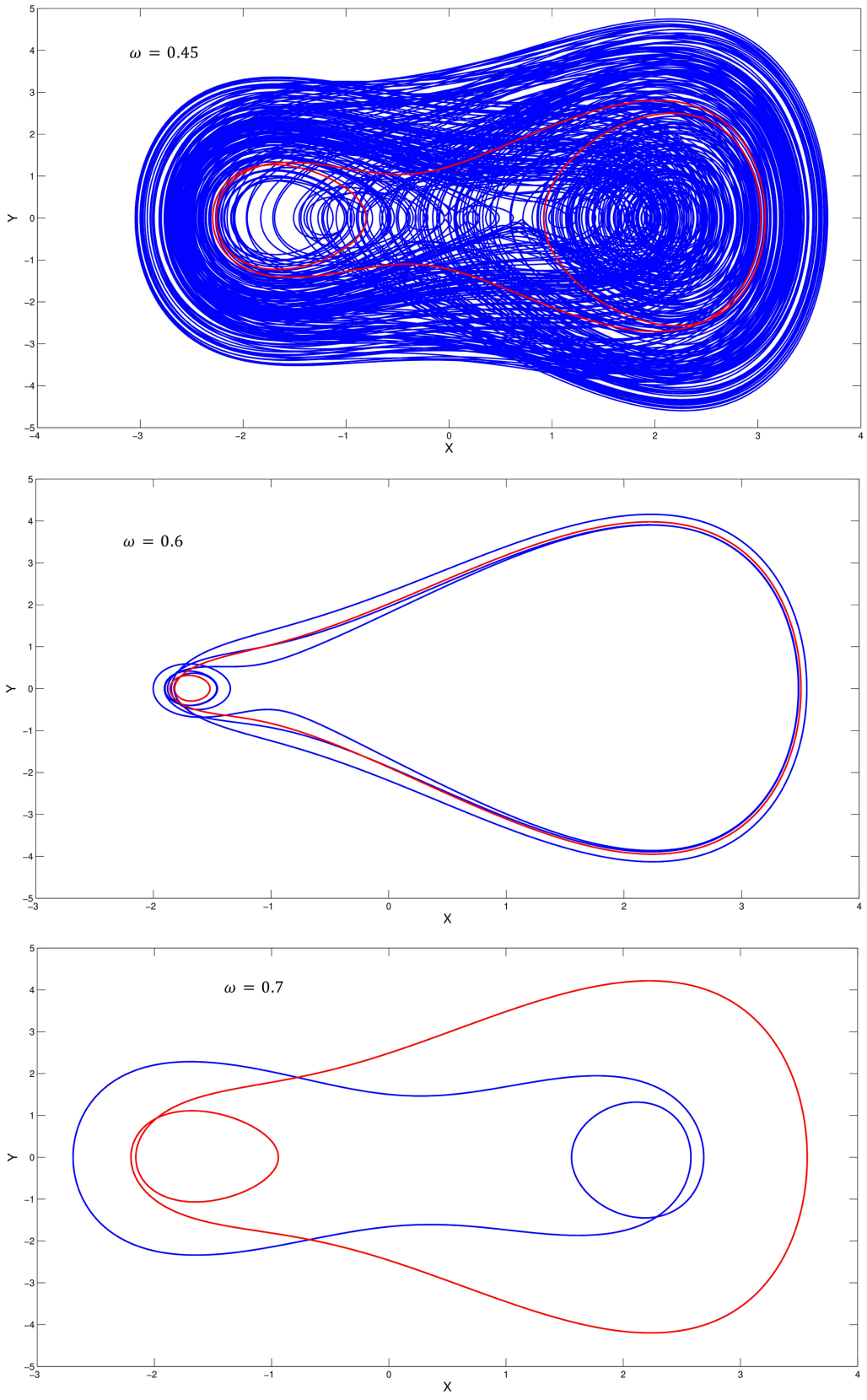

Figure 15. Coexisting attractor behaviors of the system with four different values of $\omega = 0.25$. The other parameter values of **Figure 9** are kept constant.

5. Coexisting Attractors Behaviors

In this section, we numerically investigate the phenomenon of coexistence of attractors by studying the effect of initial conditions on the dynamical behavior of the system. The blue, red, and green colors are used for initial conditions (0.5, 0.5), (0.1, 0.1), and (−2.5, 0.5), respectively. Figure 14 shows the occurrence of coexisting attractor behaviors for four different values of β_1 with $\omega = 0.25$. For instance, when $\beta_1 = -0.01$, two asymmetric secondary mixed-mode oscillations of different typologies coexist. As $\beta_1 = -0.02$, two chaotic oscillations and secondary periodic mixed-mode oscillations coexist. For $\beta_1 = 0.01$ secondary periodic mixed-mode oscillation coexists with chaotic oscillation. On the other hand, free chaotic oscillations coexist as $\beta_1 = 0.1$. We have also investigated the onset of coexisting attractor behaviors when ω evolves with the parameters of Figure 10. The results obtained are shown in Figure 15. From this figure, we notice that for $\omega = 0.26$, bistable secondary periodic mixed-mode oscillations coexist. As $\omega = 0.38$ and 0.45 chaotic oscillation coexists with 2^2MMOs and 2^1MMOs oscillations, respectively. When $\omega = 0.6$, secondary periodic mixed mode oscillation coexists with primary periodic mixed mode oscillation. On the other hand, two asymmetric primary 1^1MMOs coexist when $\omega = 0.7$.

6. Conclusion

In this paper, we investigated the existence of bursting phenomena and mixed-mode oscillations in a tree trunk structure subjected to an aerodynamic force. The results presented herein provide insight into how small initial perturbations can lead to chaotic oscillations in tree trunks. Furthermore, the global dynamic changes of our system were studied numerically using a fourth-order Runge-Kutta scheme. The results reveal that the system exhibits primary and secondary mixed-mode periodic oscillations as well as chaotic bursting oscillations. The mechanisms underlying the bursting oscillations were analyzed through bifurcation diagrams and the corresponding Lyapunov exponent diagrams. The results indicate that the bursting oscillations in our system can be classified into three categories: asymmetric fold/Hopf-fold bursting, asymmetric Hopf-fold/fold-Hopf bursting, asymmetric fold-Hopf/Hopf-fold-fold bursting, fold/Hopf-fold hysteresis bursting, and asymmetric Hopf-fold-fold/fold-Hopf bursting. Our investigation was further extended to the emergence of coexisting attractors when certain parameters, such as the motion frequency and the parametric damping coefficient, vary. Understanding mixed-mode oscillations and coexisting attractors aids in better assessing the risk of tree failure. Indeed, it shows that their response to wind can change abruptly. A single tree may transition from a low-amplitude oscillation regime to a much more violent regime due to a simple gust or perturbation. Such sudden transitions significantly increase stresses in the trunk and roots, thereby raising the risk of cracking, breakage, or uprooting. MMOs and the coexistence of attractors can help identify critical meteorological conditions that may trigger dangerous tree oscillations and evaluate tree stability based on its mechanical proper-

ties, such as mass and damping. By incorporating these nonlinear phenomena into models, it is possible to more accurately predict critical conditions and improve risk management in forestry and urban environments.

Acknowledgements

The authors thank four anonymous reviewers for their significant contributions to the success of this work.

Conflicts of Interest

The authors declare no conflicts of interest regarding the publication of this paper.

References

[1] de Langre, E. (2008) Effects of Wind on Plants. *Annual Review of Fluid Mechanics*, **40**, 141-168. https://doi.org/10.1146/annurev.fluid.40.111406.102135

[2] James, K.R., Haritos, N. and Ades, P.K. (2006) Mechanical Stability of Trees under Dynamic Loads. *American Journal of Botany*, **93**, 1522-1530. https://doi.org/10.3732/ajb.93.10.1522

[3] Schindler, D., Bauhus, J. and Mayer, H. (2012) Wind Effects on Trees. *European Journal of Forest Research*, **131**, 159-163. https://doi.org/10.1007/s10342-011-0582-5

[4] Sellier, D. (2004) Analyse numérique du comportement mécanique d'arbres sous sollicitation aérodynamique turbulente. Ph.D. Thesis, Université Sciences et Technologies Bordeaux-1. https://theses.hal.science/tel-00008956v1

[5] Dupont, S., Défossez, P., Bonnefond, J., Irvine, M.R. and Garrigou, D. (2018) How Stand Tree Motion Impacts Wind Dynamics during Windstorms. *Agricultural and Forest Meteorology*, **262**, 42-58. https://doi.org/10.1016/j.agrformet.2018.06.022

[6] Grande, E., Giordano, E. and Clementi, F. (2023) Evaluation of Dynamic Properties of Trees Subjected to Induced Vibrations. *Applied Sciences*, **13**, Article 7333. https://doi.org/10.3390/app13127333

[7] Roodbaraky, B.S.H.J. (1994) Dynamics and Aerodynamics of Deciduous Urban Trees. Ph.D. Thesis, University of Nottingham.

[8] Spatz, H.C. and Zebrowski, J. (2001) Oscillation Frequencies of Plant Stems with Apical Loads. *Planta*, **214**, 215-219. https://doi.org/10.1007/s004250100627

[9] Wood, C. (1995) Understanding Wind Forces on Trees. In: Coutts, M.P. and Grace, J., *In Wind and trees*, Cambridge University Press, 133-164.

[10] Fečkan, M. and Pospíšil, M. (2013) Bifurcation of Sliding Periodic Orbits in Periodically Forced Discontinuous Systems. *Nonlinear Analysis: Real World Applications*, **14**, 150-162. https://doi.org/10.1016/j.nonrwa.2012.05.009

[11] Yemeli Lola, M., Romanic, K. and Francois Beceau, P. (2023) Bursting Phenomenon and Chaos Phase Control in Plant Dynamics. *Complexity*, **2023**, 1-19. https://doi.org/10.1155/2023/3206434

[12] Munoz-Pacheco, J.M. and Tlelo-Cuautle, E. (2007) Synthesis of N-Scroll Attractors Using Saturated Functions from High-Level Simulation. *Journal of Physics: Conference Series*, **96**, Article 012050. https://doi.org/10.1088/1742-6596/96/1/012050

[13] Wang, Z., Abdolmohammadi, H.R., Alsaadi, F.E., Hayat, T. and Pham, V.T. (2018) A New Oscillator with Infinite Coexisting Asymmetric Attractors. *Chaos, Solitons & Fractals*, **110**, 252-258. https://doi.org/10.1016/j.chaos.2018.03.031

[14] Ando, H., Suetani, H., Kurths, J. and Aihara, K. (2012) Chaotic Phase Synchronization in Bursting-Neuron Models Driven by a Weak Periodic Force. *Physical Review E*, **86**, Article 016205. https://doi.org/10.1103/physreve.86.016205

[15] Dana, S.K., Sethia, G.C. and Sen, A. (2007) Bursting near Homoclinic Bifurcation in Two Coupled Chua Oscillators. *International Journal of Bifurcation and Chaos*, **17**, 3437-3442.

[16] Fallah, H. (2016) Symmetric Fold/Super-Hopf Bursting, Chaos and Mixed-Mode Oscillations in Pernarowski Model of Pancreatic Beta-Cells. *International Journal of Bifurcation and Chaos*, **26**, Article 1630022. https://doi.org/10.1142/s0218127416300226

[17] Wang, X.J. (1993) Genesis of Bursting Oscillations in the Hindmarsh-Rose Model and Homoclinicity to a Chaotic Saddle. *Physica D*: *Nonlinear Phenomena*, **62**, 263-274. https://doi.org/10.1016/0167-2789(93)90286-a

[18] Han, X. and Bi, Q. (2011) Bursting Oscillations in Duffing's Equation with Slowly Changing External Forcing. *Communications in Nonlinear Science and Numerical Simulation*, **16**, 4146-4152. https://doi.org/10.1016/j.cnsns.2011.02.021

[19] Wu, H., Bao, B., Liu, Z., Xu, Q. and Jiang, P. (2014) Chaotic and Periodic Bursting Phenomena in a Memristive Wien-Bridge Oscillator. *Nonlinear Dynamics*, **83**, 893-903. https://doi.org/10.1007/s11071-015-2375-8

[20] Narasimha, R. and Kailas, S. (1990) Some Ecological Studies on Distribution of Bryophytes and Its Applications Invisakhapatnam District, Eastern Ghats of India. *Atmospheric Environment*, **241**, 1635-1645.

[21] Shah, D.A. and Antonia, R.A. (1989) Scaling of the "Bursting" Period in Turbulent Boundary Layer and Duct Flows. *Physics of Fluids A*: *Fluid Dynamics*, **1**, 318-325. https://doi.org/10.1063/1.857450

[22] Avrutin, V., Zhusubaliyev, Z.T., Saha, A., Banerjee, S., Sushko, I. and Gardini, L. (2016) Dangerous Bifurcations Revisited. *International Journal of Bifurcation and Chaos*, **26**, Article 1630040. https://doi.org/10.1142/s0218127416300408

[23] Mak, A.F.T., Yu, Y., Kwan, L.P.C., Sun, L. and Tam, E.W.C. (2011) Deformation and Reperfusion Damages and Their Accumulation in Subcutaneous Tissues during Loading and Unloading: A Theoretical Modeling of Deep Tissue Injuries. *Journal of Theoretical Biology*, **289**, 65-73. https://doi.org/10.1016/j.jtbi.2011.08.022

[24] Berenstein, I. and De Decker, Y. (2015) Spatiotemporal Chaos from Bursting Dynamics. *The Journal of Chemical Physics*, **143**, Article 064105. https://doi.org/10.1063/1.4927911

[25] Gu, H. and Xiao, W. (2014) Difference between Intermittent Chaotic Bursting and Spiking of Neural Firing Patterns. *International Journal of Bifurcation and Chaos*, **24**, Article 1450082. https://doi.org/10.1142/s0218127414500825

[26] Rinzel, J. (1985) Bursting Oscillation in an Excitable Membrane Model. In: *Ordinary and Partial Differential Equations*, Springer, 304-316.

[27] Ma, X. and Cao, S. (2018) Bursting Oscillations in Shimizu-Morioka System with Slow-Varying Periodic Excitation. *Shock and Vibration*, **2018**, Article 5207910. https://doi.org/10.1155/2018/5207910

[28] Low, P.S. and Merida, J.R. (1996) The Oxidative Burst in Plant Defense: Function and Signal Transduction. *Physiologia Plantarum*, **96**, 533-542. https://doi.org/10.1111/j.1399-3054.1996.tb00469.x

[29] Scheel, D. (1998) Resistance Response Physiology and Signal Transduction. *Current Opinion in Plant Biology*, **1**, 305-310. https://doi.org/10.1016/1369-5266(88)80051-7

[30] Kingston, S.L. and Thamilmaran, K. (2017) Bursting Oscillations and Mixed-Mode Oscillations in Driven Liénard System. *International Journal of Bifurcation and Chaos*, **27**, Article 1730025. https://doi.org/10.1142/s0218127417300257

[31] Upadhyay, R.K., Mondal, A. and Teka, W.W. (2017) Mixed Mode Oscillations and Synchronous Activity in Noise Induced Modified Morris-Lecar Neural System. *International Journal of Bifurcation and Chaos*, **27**, Article 1730019. https://doi.org/10.1142/s0218127417300191

[32] Han, X., Bi, Q., Zhang, C. and Yu, Y. (2014) Study of Mixed-Mode Oscillations in a Parametrically Excited Van Der Pol System. *Nonlinear Dynamics*, **77**, 1285-1296. https://doi.org/10.1007/s11071-014-1377-2

[33] Budroni, M.A., Garroni, S., Mulas, G. and Rustici, M. (2017) Bursting Dynamics in Molecular Hydrogen Generation via Sodium Borohydride Hydrolysis. *The Journal of Physical Chemistry C*, **121**, 4891-4898. https://doi.org/10.1021/acs.jpcc.6b12797

[34] Ren, J., Gao, J.Z. and Yang, W. (2013) The Application of Oscillating Chemical Reactions to Analytical Determinations. *Central European Journal of Chemistry*, **11**, 1023-1031.

[35] Peng, M., Zhang, Z.D., Lim, C.W. and Wang, X.D. (2018) Hopf Bifurcation and Hybrid Control of a Delayed Ecoepidemiological Model with Nonlinear Incidence Rate and Holling Type II Functional Response. *Mathematical Problems in Engineering*, **2018**, 1-12. https://doi.org/10.1155/2018/6052503

[36] Kuwamura, M. and Chiba, H. (2009) Mixed-Mode Oscillations and Chaos in a Prey-Predator System with Dormancy of Predators. *Chaos*, **19**, Article 043121. https://doi.org/10.1063/1.3270262

[37] Shimizu, K., Sekikawa, M. and Inaba, N. (2015) Experimental Study of Complex Mixed-Mode Oscillations Generated in a Bonhoeffer-Van Der Pol Oscillator under Weak Periodic Perturbation. *Chaos*, **25**, Article 023105. https://doi.org/10.1063/1.4907741

[38] Chakraborty, S. and Dana, S.K. (2010) Shil'nikov Chaos and Mixed-Mode Oscillation in Chua Circuit. *Chaos*, **20**, Article 023107. https://doi.org/10.1063/1.3378112

[39] Kpomahou, Y.J.F., Adéchinan, J.A., Ngounou, A.M. and Yamadjako, A.E. (2022) Bursting, Mixed-Mode Oscillations and Homoclinic Bifurcation in a Parametrically and Self-Excited Mixed Rayleigh-Liénard Oscillator with Asymmetric Double Well Potential. *Pramana*, **96**, 1-16. https://doi.org/10.1007/s12043-022-02412-0

[40] Talla, P.K., Mabekou, S.T. and Moukouri, J. (2013) The Stochastic Dynamic and Nonlinear Oscillations of a Plant under Wind Effects. *Far East Journal of Dynamical Systems*, **22**, 55-85.

[41] Doaré, O., Moulia, B. and de Langre, E. (2004) Effect of Plant Interaction on Wind-Induced Crop Motion. *Journal of Biomechanical Engineering*, **126**, 146-151. https://doi.org/10.1115/1.1688773

[42] Py, C., de Langre, E. and Moullia, B. (2006) A Frequency Lock-In Mechanism in the Interaction between Wind and Crop Canopies. *Journal of Fluid Mechanics*, **568**, 425-449. https://doi.org/10.1017/s0022112006002667